YMTHE, Volume *26*

Supplemental Information

The Neurotropic Properties of AAV-PHP.B Are Limited to C57BL/6J Mice

Juliette Hordeaux, Qiang Wang, Nathan Katz, Elizabeth L. Buza, Peter Bell, and James M. Wilson

Supplemental Data

Supplemental Figures

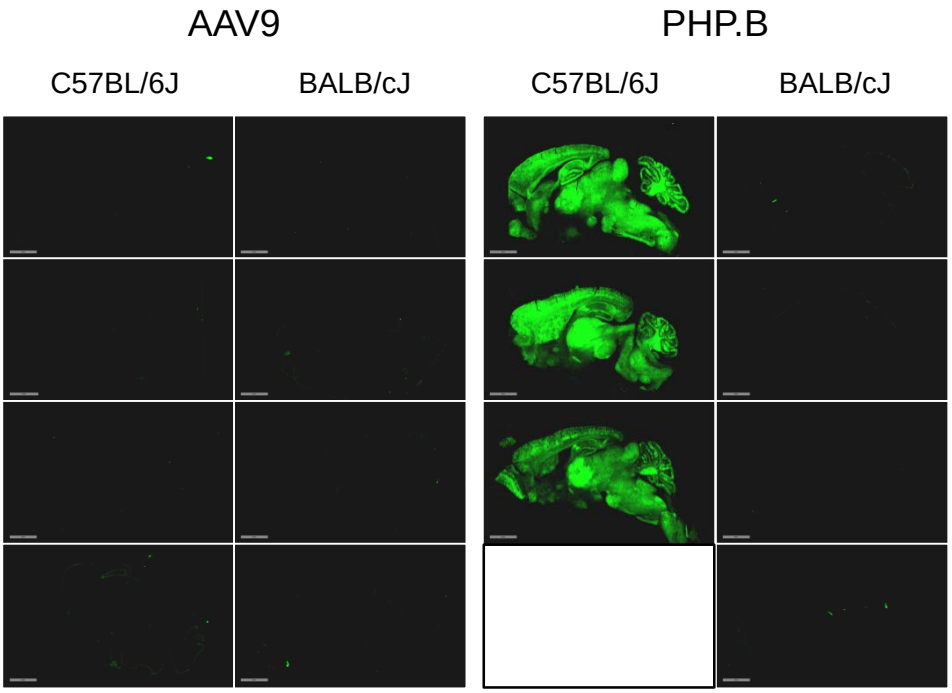

Supplemental Figure 1. Direct observation of GFP in the brain of individual AAV9 and PHP.B-injected mice. After systemic administration of $5x10^{13}$ GC/kg to adult mice, GFP expression is minimal in AAV9-injected mice and in PHP.B-injected BALB/cJ mice at 21 days post injection. GFP expression is marked in C57Bl6 PHP.B-injected mice.Individual variations are minimal. Data for one PHP.B-injected C57BL/6J animal is not available due to a failed injection. Scale bars 2mm.

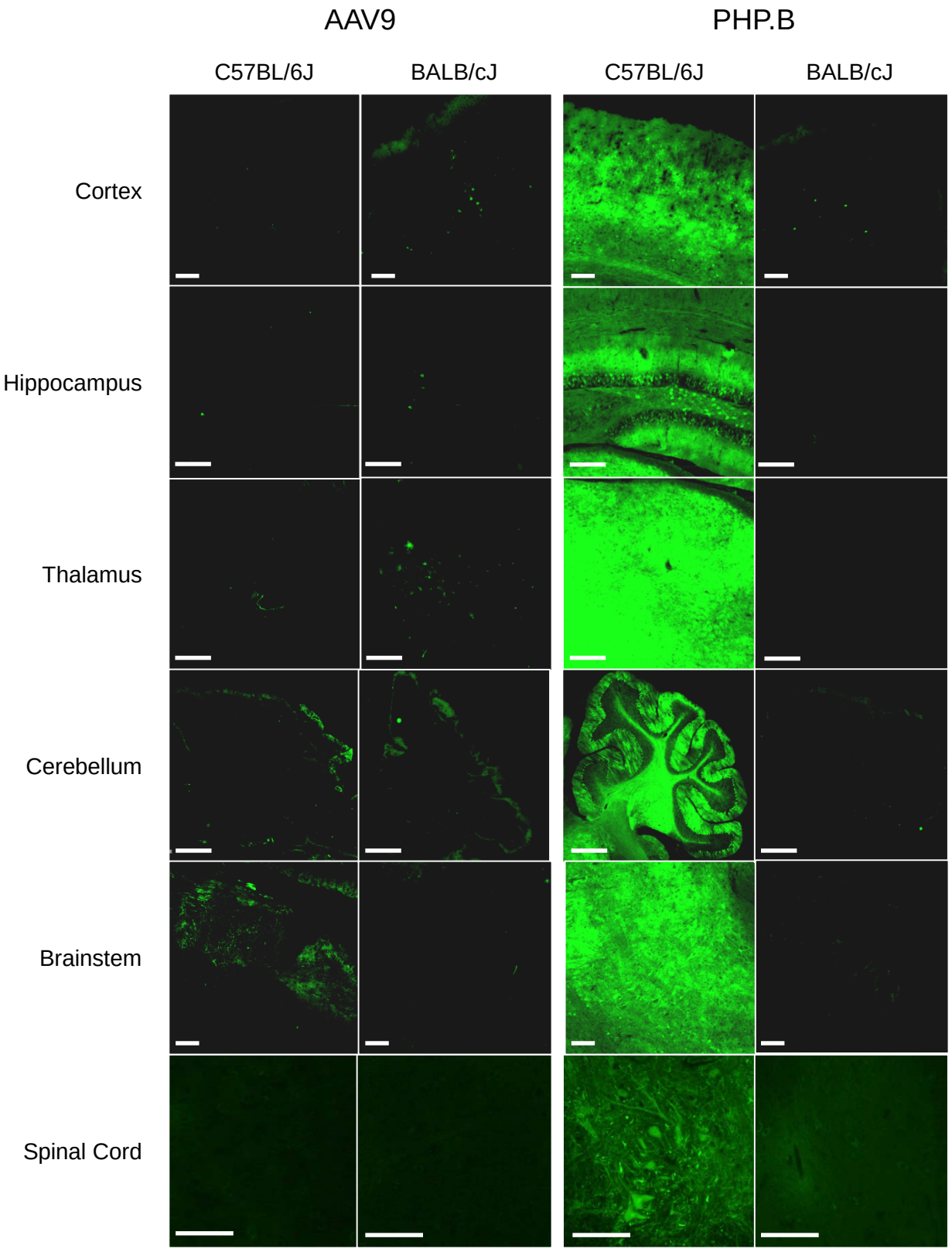

Supplemental Figure 2. Direct observation of GFP in the brain of AAV9 and PHP.B-injected mice at high magnification. Mice were injected in the tail vein with $5x10^{13}$ GC/kg of AAV9 or AAV-PHP.B encoding GFP. 21 days pi, all CNS regions are highly transduced after PHP.B injection in C57BL/6J mice: cortex (scale bar 100 µm), hippocampus (scale bar 200 µm), thalamus (scale bar 200 µm), cerebellum (scale bar 700 µm), brainstem (scale bar 150 µm), and spinal cord (motor neurons, scale bar 100 µm). PHP.B-driven GFP expression is marked in C57BL/6J and almost absent in BALB/cJ mice. With AAV9, no significant difference is seen in C57BL/6J and BALB/cJ mice.

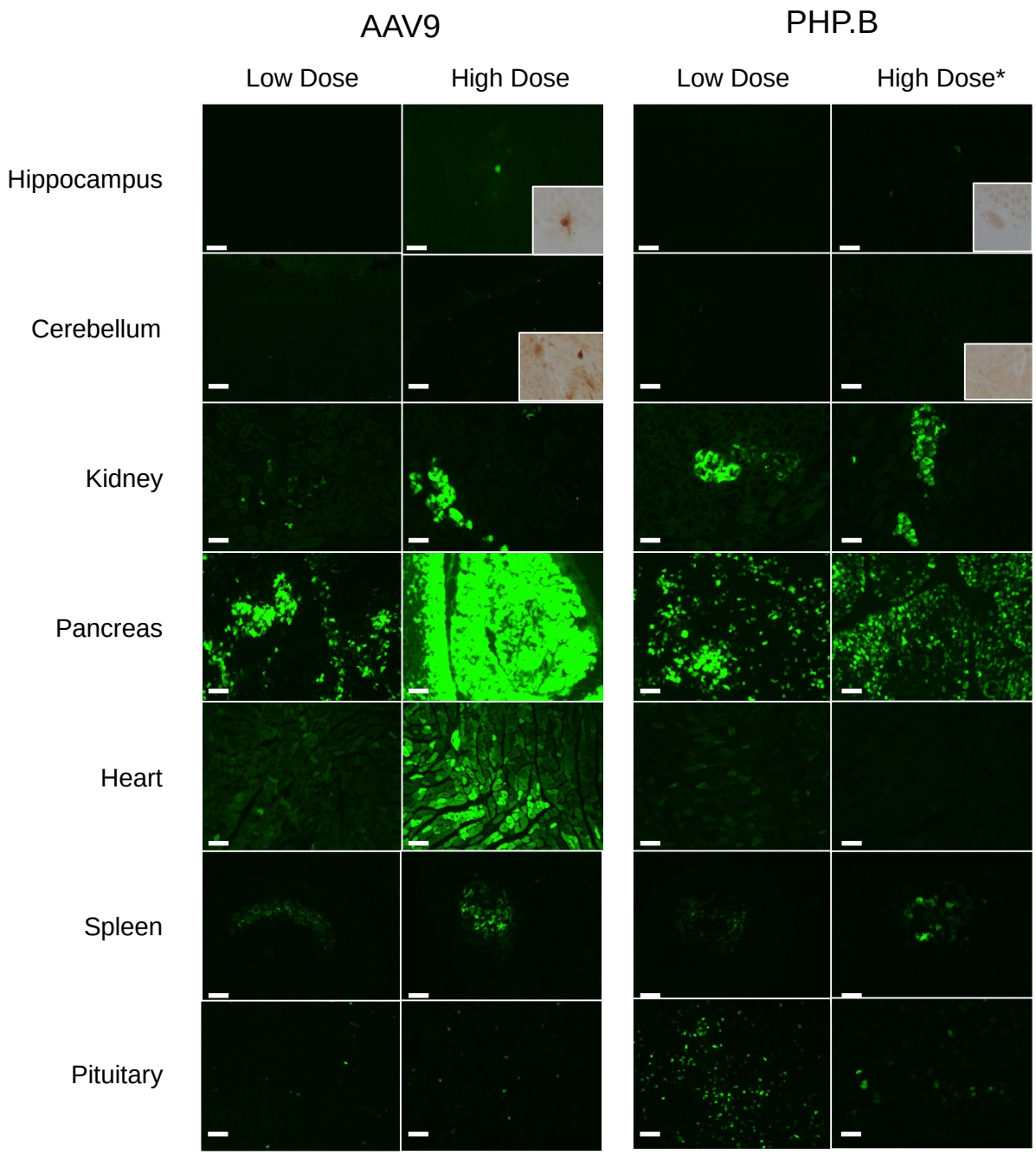

Supplemental Figure 3. AAV9 and PHP.B-mediated gene transfer in additional tissues of nonhuman primates. Low dose is $2x10^{13}$ GC/kg and high dose is $7.5x10^{13}$ GC/kg. Hippocampus, cerebellum, kidney, pancreas, heart, spleen, and pituitary are depicted. Inset images show GFP immunohistochemistry in the high dose animals. *Euthanized 5 days post injection; all others euthanized 21 days post injection. AAV9 drives dose-dependent GFP expression that is markedly more efficient in organs that lay outside of the blood-brain barrier. The expression profile is similar in PHP.B, although high-dose expression data are not directly comparable due to the shorter post injection time. Scales bars 100 µm.

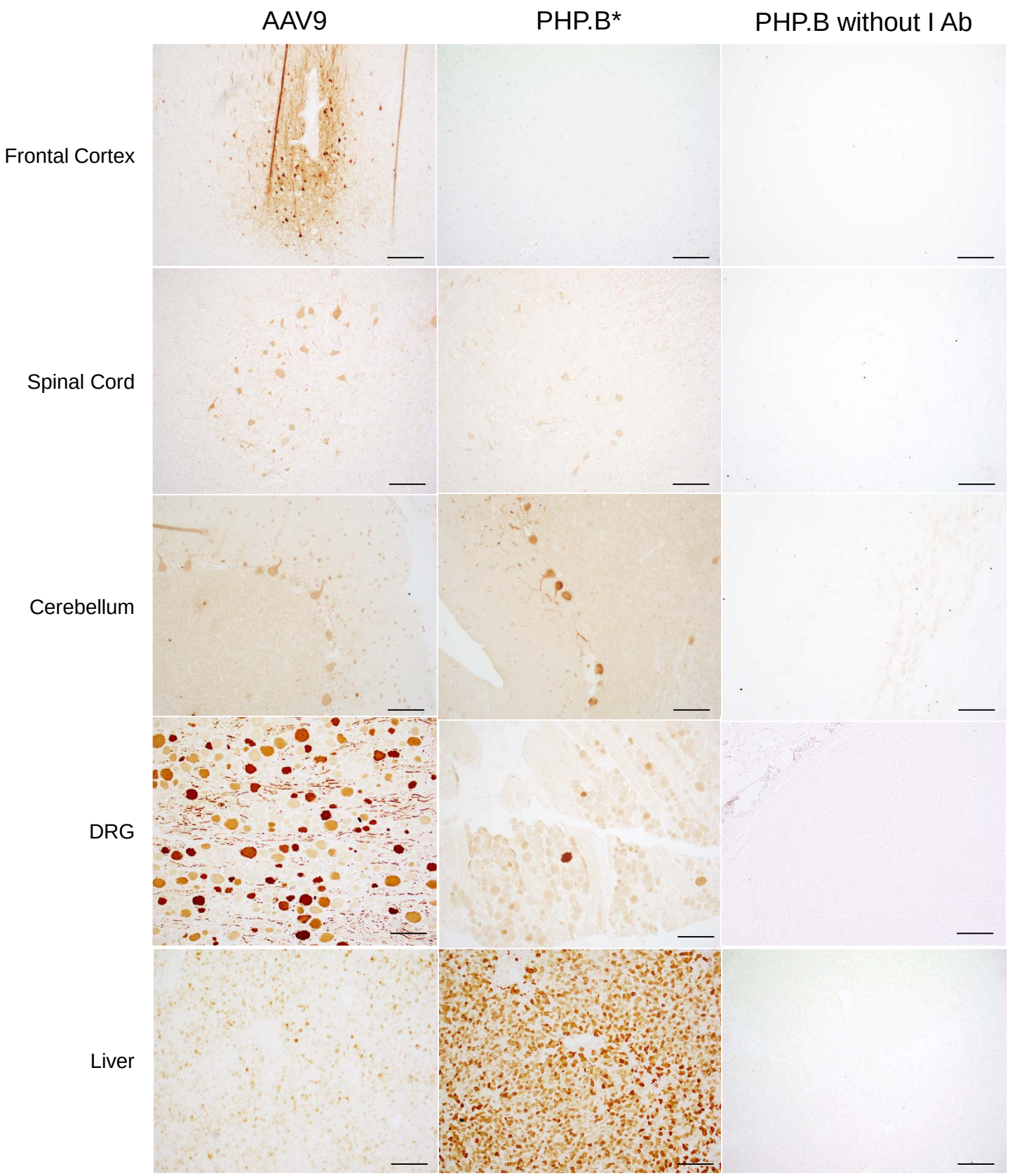

Supplemental Figure 4. GFP immunohistochemistry in high-dose nonhuman primates injected with AAV9 and PHP.B vectors. Frontal cortex, spinal cord (anterior horns), cerebellum, dorsal root ganglia (DRG), and liver are depicted. *Euthanized 5 days post injection. Positive (brown) neurons are seen in the AAV9 high-dose animal in the frontal cortex (perivascular pattern), anterior horns of the spinal cord, cerebellum (granular layer and Purkinje cells) and DRG. In the PHP.B animal, expression is suboptimal at this early timepoint and only visible in some Purkinje cells and DRG neurons. Scale bars 200 µm.

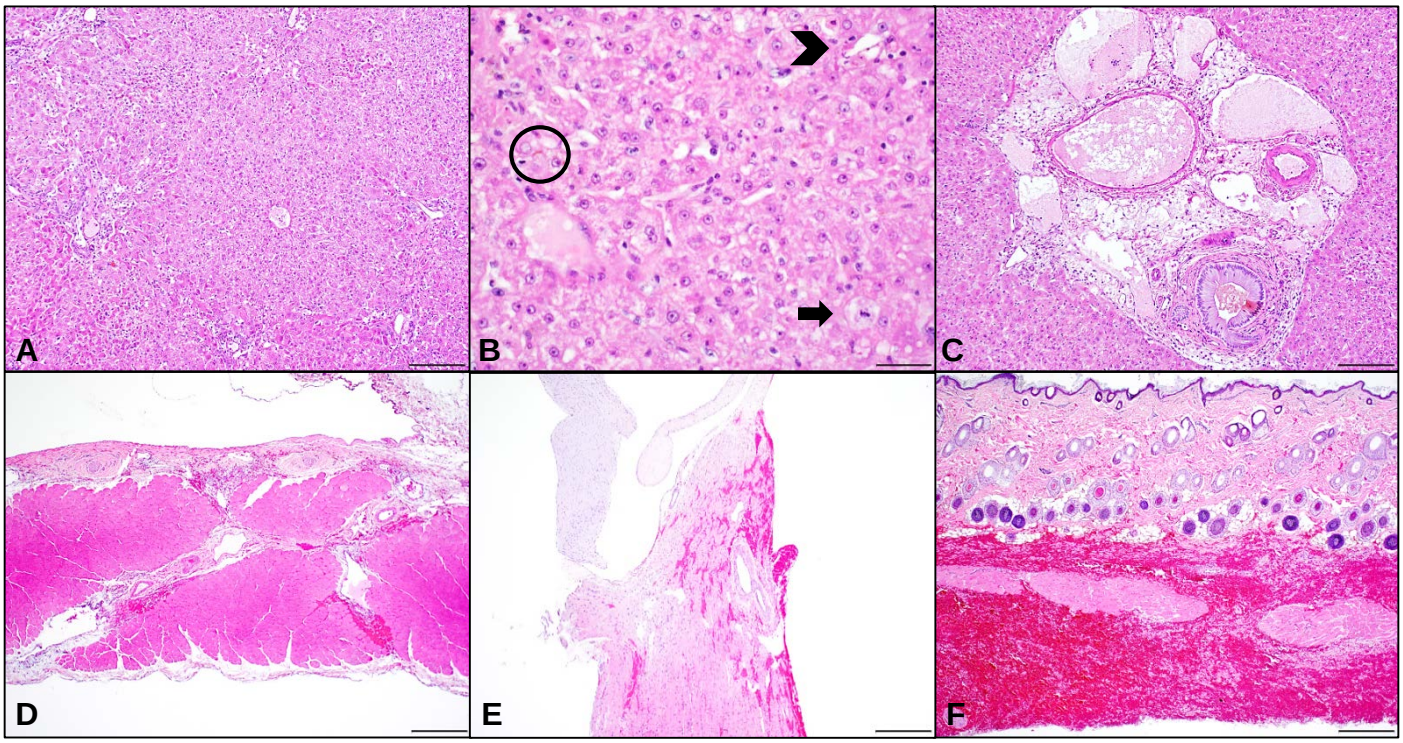

Supplemental Figure 5. Histopathology of high-dose PHP.B NHP (RA2152). The histology findings were most significant in liver (**A-C**) and consisted of marked multifocal single hepatocellular necrosis and degeneration, most prominently centered on portal regions with occasional bridging (**A**, scale bar 200 µm). Along with individual hepatocellular necrosis (*arrowhead*), there were also increased numbers of mitotic figures (*arrow*) indicative of regeneration (**B**, scale bar 50 µm). Both canalicular (**B**, circle) and ductal (**C**, scale bar 200 µm) bile stasis were prominent. Portal areas were edematous with dilated portal veins and lymphatics (**C**). Acute hemorrhage was observed in the diaphragm (**D**, scale bar 500 µm), heart (**E**, scale bar 500 µm), and subcutis (**F**, scale bar 200 µm).

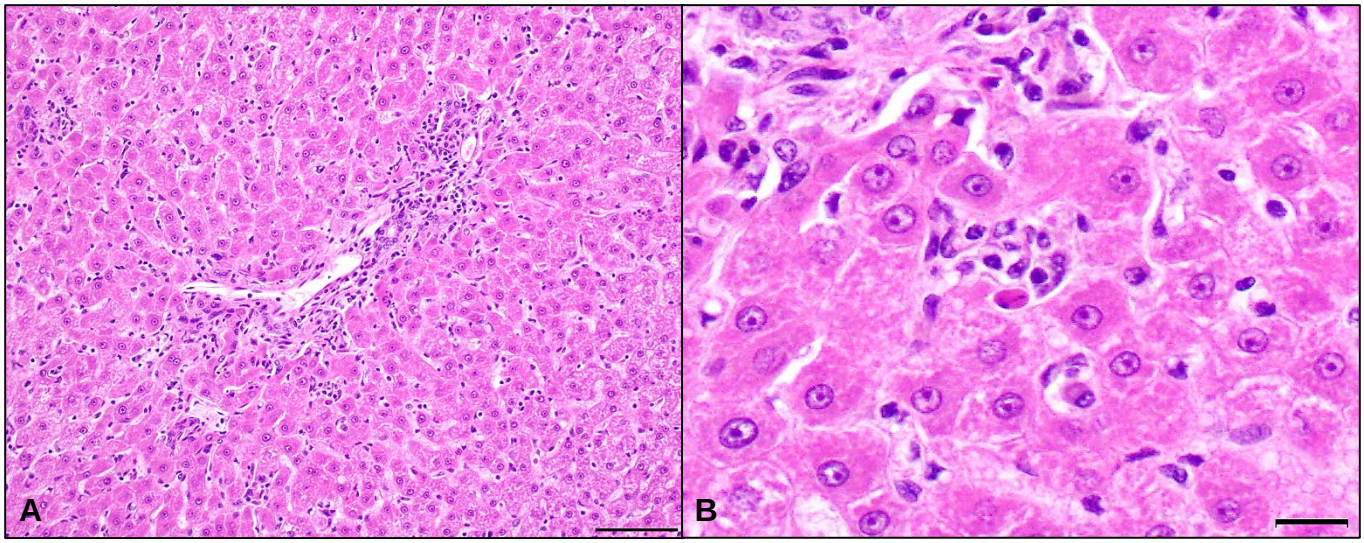

Supplemental Figure 6: Histopathology of high-dose AAV9 NHP (RA2235). The histopathology findings in animal RA2235 consisted of minimal mononuclear cell infiltrates within the liver (**A**-**B**). The mononuclear cell infiltrates in the liver were within portal and periportal areas (**A**, scale bar 100 µm) and occasionally associated with single hepatocellular necrosis (**B**, scale bar 20 µm). The mononuclear cell infiltrates likely corresponded to an immune (e.g. T-lymphocyte) response related to vector expression.

Supplemental Table 1. Nonhuman primates dosed with systemic AAV9 and PHP.B.

Animal	**Gender, age**	**Weight**	**Vector**		**Outcome**
RA2172	Female, 4 years	5.3 kg	AAV9.CB7.eGFP.WPRE.rBG	2e13 GC/kg	Scheduled euthanasia D21
RA2235	Male, 4 years	6.7 kg	AAV9.CB7.eGFP.WPRE.rBG	7.5e13 GC/kg	Scheduled euthanasia D21
RA2145	Female, 4 years	4.8 kg	AAV-PHP.B.CB7.eGFP.WPRE.rBG	2e13 GC/kg	Scheduled euthanasia D21
RA2152	Female, 4 years	5.9 kg	AAV-PHP.B.CB7.eGFP.WPRE.rBG	7.5e13 GC/kg	Hemorrhagic diathesis ; Unscheduled euthanasia D5

Supplemental Table 2. Clinical pathology, PHP.B (RA2152) and AAV9 (RA2235) high dose animals.

	Parameter	Day 0, prior to dosing	Day 3	Day 5	Day 7	Day 14	Day 21
RA2152 PHP.B	White blood cells 10^3/µL	12.2	3	3.8	N/A	N/A	N/A
	Red blood cells 10^6/µL	4.5	4.8	3			
	Hemoglobin g/dL	11.6	12.5	7.3			
	Hematocrit %	38	37	23			
	Mean corpuscular volume fl/cell	85	77	75			
	Mean corpuscular hemoglobin pg/cell	25.6	26.2	24.2			
	Mean corpuscular hemoglobin g/dL	30	34	32			
	Platelets 10^3/µL	247	46	18			
	Neutrophils cell/µL	8,662	1200	1748			
	% neutrophils	71	40	46			
	Bands cell/µL	0	0	0			
	% band cells	0	0	0			
	Lymphocytes cell/µL	2,928	1,710	1,368			
	% Lymphocytes	24	57	36			
	Monocytes cell/µL	244	60	380			
	% monocytes	2	2	10			
	Eosinophils cell/µL	366	30	304			
	% eosinophils	3	1	8			
	Basophils cell/µL	0	0	0			
	% basolphils	0	0	0			
	Total protein g/dL	6.6	5.9	5.3			
	Albumin g/dL	4.2	3.2	3			
	Globulin g/dL	2.4	2.7	2.3			
	A\G ratio	1.8	1.2	1.3			
	AST IU/ L	19	740	242			
	ALT IU/ L	30	1,145	736			
	ALP IU/ L	311	680	723			
	GGTP IU/ L	61	123	90			
	Total bilirubin mg/dL	0.2	2	2.1			
	Urea (BUN) mg/dL	17	17	14			
	Creatinine mg/dL	0.5	0.4	0.3			
	BUN/CREA Ratio	34	43	47			
	Ph mg/dL	5.3	4.5	4			
	Glucose mg/dL	57	92	77			
	Ca mg/dL	9.2	7.9	7.9			
	Mg mg/dL	1.5	1.8	1.6			
	Na mmol/L	145	139	141			
	K mmol/L	3.1	3.6	4.2			
	NA/K ratio	47	39	34			
	Chloride mmol/L	108	105	106			
	Cholesterol	117	99	108			
	Triglycerides	49	19	27			
	Amylase U/L	304	194	248			
	Precision Pancreas specific lipase U/L	29	26	18			
	Creatine phosphokinase U/L	535	124	857			
	Prothrombin time sec	9.5	11.9	12			
	Partial thromboplastin time sec	25.4	31.5	29.8			
	Fibrinogen mg/dL	136	134	79			
	D-dimer ng/mL	42	147	20			
RA2235 AAV9	White blood cells 10^3/µL	7.2	7	N/A	12	6.3	6
	Red blood cells 10^6/µL	5.7	5.4		5.6	5.6	5.3

	Hemoglobin g/dL	13.1	12.9		12.8	12.6	12.4
	Hematocrit %	46	42		43	44	41
	Mean corpuscular volume fl/cell	80	77		76	78	78
	Mean corpuscular hemoglobin pg/cell	23	23.7		22.8	22.7	23.5
	Mean corpuscular hemoglobin g/dL	29	31		30	29	30
	Platelets 10^3/µL	361	270		261	377	428
	Neutrophils cell/µL	3168	3640		5160	2898	1260
	% neutrophils	44	52		43	46	21
	Bands cell/µL	0	0		0	0	0
	% band cells	0	0		0	0	0
	Lymohocytes cell/µL	3672	3290		5760	2898	4140
	% Lymphocytes	51	47		48	46	7
	Monocytes cell/µL	288	70		840	441	420
	% monocytes	4	1		7	7	7
	Eosinophils cell/µL	72	0		240	63	180
	% eosinophils	1	0		2	1	3
	Basophils cell/µL	0	0		0	0	0
	% basolphils	0	0		0	0	0
	Total protein g/dL	6.5	6.6		6.4	6.2	5.9
	Albumin g/dL	4.4	3.9		3.9	3.9	3.7
	Globulin g/dL	2.1	2.7		2.5	2.3	2.2
	A\G ratio	2.1	1.4		1.6	1.7	1.7
	AST IU/ L	43	171		41	551	54
	ALT IU/ L	34	140		118	782	231
	ALP IU/ L	608	574		508	640	748
	GGTP IU/ L	77	85		80	135	142
	Total bilirubin mg/dL	0.1	0.1		0.2	0.4	0.3
	Urea (BUN) mg/dL	22	19		19	18	17
	Creatinine mg/dL	0.6	0.6		0.6	0.6	0.5
	BUN/CREA Ratio	37	32		32	30	34
	Ph mg/dL	7.1	6.1		5.6	6.8	6.3
	Glucose mg/dL	75	144		118	76	98
	Ca mg/dL	9.3	9.4		9.1	9	9.7
	Mg mg/dL	1.6	1.5		1.5	1.4	1.4
	Na mmol/L	146	141		143	147	144
	K mmol/L	3.9	4.1		2.8	3.7	3.7
	NA/K ratio	37	34		51	40	39
	Chloride mmol/L	108	107		107	107	106
	Cholesterol	137	126		139	142	175
	Triglycerides	51	138		73	50	137
	Amylase U/L	262	258		283	204	258
	Precision Pancreas specific lipase U/L	45	44		34	29	36
	Creatine phosphokinase U/L	2383	141		123	171	134
	Prothrombin time sec	10	9.4		8.4	10.4	10.5
	Partial thromboplastin time sec	24.4	23.1		22.5	23.4	25.8
	Fibrinogen mg/dL	181	224		198	170	116
	D-dimer ng/mL	41	47		24	92	67

N/A not applicable

Clinical Case Description

A summary of the clinical findings for NHPs that received 7.5E13 GC/kg of AAV9 or PHP.B is provided below. Test article (AAV-PHP.B.CB7.CI.eGFP.WPRE.rBG; group 2) or reference article (AAV9.CB7.CI.eGFP.WPRE.rBG; group 1) was administered at a dose of 7.5E13 GC/kg IV to rhesus macaques (*Macaca mulatta*), RA2152 and RA2235, respectively (Supplemental Table 1). Necropsies were scheduled for 21 ±1 days post vector administration; however, animal RA2152 (PHP.B; group 2) was euthanized on Day 5 due to clinical signs and bloodwork abnormalities. Subsequently, direct histological comparison of these 2 vectors was not possible. The clinical pathology data for both animals are depicted in Supplemental Table 2.

Animal RA2235 (group 1), which received AAV9, was clinically normal throughout the study and necropsied according to protocol on Day 22. Grossly, no significant study-related findings were observed. No significant abnormalities were noted on serial complete blood counts (CBC); however, serum chemistry on Day 3 showed elevated (~200 U/L) liver enzymes (AST/ALT) and were trending down until Day 14. On Day 14, aspartate aminotransferase (AST) and alanine aminotransferase (ALT) spiked to ~500-800 U/dL and returned to normal levels by Day 22. Histologically within the liver there was minimal mononuclear cell infiltrates, primarily within portal and periportal regions that were occasionally associated with single hepatocellular necrosis (Supplemental Fig. 6). Minimal to mild mononuclear cell infiltrates were also observed in the heart and skeletal muscle of the diaphragm, right biceps brachii, right quadriceps femoris, and left gastrocnemius muscles (data not shown). Given the level of GFP expression in the heart and skeletal muscle, an association between these infiltrates and AAV9 vector cannot be completely ruled out; however, similar infiltrates have been reported as incidental or background findings in nonhuman primates[1]. However, the lack of concurrent sham-treated control animals renders the interpretation of these infiltrates difficult. Additionally, minimal multifocal perivascular mononuclear cell infiltrates were in brain, and the relationship of these findings to the reference article was uncertain. The dorsal root ganglia (DRG) had minimal mononuclear cell infiltrates with occasional neuronal cell body degeneration; however, all spinal cord segments were histologically unremarkable.

Animal RA2152 (group 2), which received PHP.B, had icteric serum on Day 3 and serum chemistry revealed an elevated AST (740 IU/L; x40 baseline), ALT (1,145 IU/L; x40 baseline) and total bilirubin (2 mg/dL; x10 baseline). On complete blood count (CBC), leukopenia ($3x10^3$/uL; x4 decrease / baseline) and thrombocytopenia ($46x10^3$/uL; x5 decrease / baseline) were noted. D-dimers (147 ng/dL) were increased on coagulation panel relative to baseline (Day 0, 42 ng/mL). Prothrombin time (PT, 11.9 sec) and partial thromboplastin time (PTT; 31.5 sec) were slightly increased compared to baseline (Day 0, PT 9.5 sec and PTT 25.4 sec); however, they were within reference range. Although behaviorally normal, the animal received IV fluids, preventative anti-emetic, and corticosteroids. On Day 4, petechial to ecchymotic to suffusive cutaneous hemorrhage was noted on the ventral and lateral abdomen and by Day 5 spread from the ventral abdomen to the left dorsum and right axillary region. While behaviorally normal, the animal was euthanized on Day 5 according to study protocol due to worsening cutaneous hemorrhage and anemia (HCT 20%), which was possibly indicative of bleeding to a coagulopathy. In addition to the skin lesions, the abdominal cavity contained approximately 30-35 mL of serosanguineous fluid. The cranial and caudal mediastinum along with the abdominal mesentery contained regional acute hemorrhage. The liver was diffusely tan and friable with an accentuated lobular pattern. Terminal clinical pathology (Day 5) data revealed a marked thrombocytopenia and stable leukopenia. Serum chemistry showed improvement of liver enzymes (AST 242 IU/L and ALT 736 IU/L) and stable total bilirubin (2.1 mg/dL). PT and PTT remained stable on coagulation panel; however, fibrinogen (79 mg/dL) was decreased compared to baseline (Day 0, 136 mg/dL) and Day 3 (134 mg/dL). The histologic findings consisted of acute hemorrhage within the diaphragm, heart, and subcutis (Supplemental Fig. 5). The gross lesions within the liver corresponded histologically to marked multifocal single hepatocellular necrosis and degeneration, most prominently centered on portal regions with occasional bridging. The necrotic hepatocytes were occasionally clustered into small aggregates. The portal areas were edematous with dilated portal veins and lymphatics. Bile ducts contained inspissated bile along with prominent canalicular bile plugs, indicative of cholestasis. Throughout

the hepatic parenchyma, there were increased numbers of mitotic figures, consistent with regeneration. No significant cellular infiltrates were observed in the liver or any other tissue examined.

A Luminex cytokine panel on serum from animal RA2152 showed no significant elevations for the majority of cytokines, except vascular endothelial growth factor (VEGF; Day 7, x10) and monocyte chemoattractant protein-1 (MCP-1; Day 3, x2). The Luminex results are not supportive of a systemic inflammatory or innate immune response; however, the treatment with corticosteroids (Day 3; 10 mg/kg) may have had an effect. Neutralizing antibody (NAb) titers for anti-AAV9/anti-PHP.B were performed for both animals. Baseline AAV9 neutralizing antibody titers were below the limit of detection (< 1:5) for both animals, while PHP.B total binding antibody titer was 1:800 for animal RA2152 and 1:40 for animal RA2135.

While the inciting cause of morbidity in animal RA2152 was likely vector-related, the mechanism is not well understood. Proposed pathologic mechanisms include primary liver injury due to AAV particles or genomes or cytokine-induced endothelial cell activation within the liver microvasculature with subsequent coagulation activation, and/or localized antigen-antibody sinusoidal endothelial cell injury. Other possibilities including systemic inflammatory conditions such as systemic endothelial activation/damage or antigen-antibody mediated platelet destruction. Individual genetic variability likely played a role as animal RA2145 (low dose, 2E13 GC/kg, PHP.B) had a similarly high vector genome distribution to the liver but did not experience significant liver injury or endothelial cell activation. While both animals were negative for NAbs to the respective vectors prior to treatment, the level of binding antibody to PHP.B in animal RA2152 was higher than binding antibody to AAV9 in RA2235. It is possible that AAV immune complexes caused by the higher binding antibodies in RA2152 may have contributed to toxicity.

Materials and Methods

Vectors

EGFP was cloned into an expression construct containing a chicken β-actin promoter, cytomegalovirus (CMV) enhancer, intron, and rabbit β-globin (rBG) polyadenylation sequence. The expression constructs were flanked by AAV2 inverted terminal repeats. The PHP.B *trans* plasmid[2] was constructed with QuikChange Lightning Site-Directed Mutagenesis Kit (Agilent Technologies, CA) on AAV9 trans plasmid. AAV vectors were manufactured by Penn Vector Core with iodixanol gradient method.[3] The purified vectors were titrated 3 times with Droplet Digital PCR[4] plus proteinase K pre-treatment, and the average of the 3 titers was used. The lots injected to NHPs had a purity of 100% and undetected endotoxin levels (<1.0 EU/mL).

Animal Procedures and Histology

All animal protocols were approved by the Institutional Animal Care and Use Committee of the University of Pennsylvania. C56BL/6J (stock #000664), BALB/cJ (#000651), and CB6F1/J (#100007) were purchased from The Jackson Laboratory. Mice received 1×10^{12} GC (5×10^{13} GC/kg) of AAV9 or PHP.B in 0.1 mL via the lateral tail vein and were euthanized by inhalation of CO_2 21 days post injection. Tissues were promptly collected, half was snap-frozen on dry ice (biodistribution), and half was immersion-fixed in 10% neutral formalin, cryo-preserved in sucrose, frozen in OCT, and sectioned with a cryostat for GFP direct observation and whole-slide scanning for GFP quantification. Four mice of each strain were injected with each vector and used for quantification of vector genome and GFP expression in tissues. A total of 8 AAV9 C57BL/6J, 8 AAV9 BALB/cJ, 12 PHP.B C57BL/6J, 12 PHP.B BALB/cJ, and 4 PHP.B CB6F1/J were used for the quantification of genome copies in the brain.

Adult (4 years old) rhesus macaques were purchased from Covance (Table S1). They received 2×10^{13} GC/kg (low dose, n = 1 per vector) or 7.5×10^{13} GC/kg (high dose, n = 1 per vector) of AAV9 or PHP.B in 10 mL via the saphenous vein under sedation (intramuscular dexmedetomidine with ketamine). All but one animal (see clinical case description) was euthanized 21 days post injection by barbiturate overdose after anesthesia. The PHP.B high-dose animal was euthanized due to clinical condition 5 days post injection. Tissues were promptly collected, some were snap-frozen on dry ice (biodistribution), and some were immersion-fixed in 10% neutral formalin, cryo-preserved in sucrose, frozen in OCT, and sectioned with a cryostat for GFP direct observation and whole-slide scanning for GFP quantification. In addition, tissues were sampled for paraffin embedding, H&E staining, and GFP immunohistochemistry in the 2 high-dose animals.

GFP Expression

To observe direct GFP fluorescence, tissue samples were fixed in formalin for about 24 hr, briefly washed in PBS, equilibrated sequentially in 15% and 30% sucrose in PBS until sinking to the bottom of the container, and finally frozen in OCT embedding medium for the preparation of cryosections. Sections were mounted in Fluoromount G containing DAPI (Electron Microscopy Sciences, Hatfield, PA) as nuclear counterstain.

GFP immunohistochemistry was performed on paraffin-embedded tissue samples. Sections were deparaffinized with ethanol and xylene, boiled for 6 min in 10 mM citrate buffer (pH 6.0) for antigen retrieval, treated sequentially with 2% H_2O_2 (15 min), avidin/biotin blocking reagents (15 min each; Vector Laboratories, Burlingame, CA), and blocking buffer (1% donkey serum in PBS + 0.2% Triton for 10 min), and followed by incubation with primary (1 hr) and biotinylated secondary antibodies (45 min; Jackson Immunoresearch, West Grove, PA) diluted in blocking buffer. As primary antibody served a rabbit serum against GFP (ab6556; Abcam, Cambridge, MA). A Vectastain Elite ABC kit (Vector Laboratories) was used following the manufacturer's instructions, with DAB as substrate, to visualize bound antibodies as brown precipitate.

Images were taken either with a Nikon Eclipse Ti-E microscope or, for low magnification pictures, as screen shots from slides scanned with an Aperio Versa fluorescence slide scanner (Leica Biosystems).

GFP Quantification

Slides of mice whole-brain, nonhuman primate frontal cortex, liver, and muscle containing cryosections were scanned with a 10× objective using an Aperio Versa fluorescence slide scanner (Leica Biosystems). Nonhuman primate DRG and lumbar spinal cord section images (10 for DRGs and 2 for lumbar spinal cord cross sections) were taken using a fluorescent microscope (Nikon Eclipse Ti-E microscope). The resulting image files were analyzed for fluorescence intensity and percentage of GFP^+ area using Halo software (Indica Labs, Corrales, NM). Briefly,

regions of interest comprising either whole sections or certain brain regions were drawn with Halo, and a threshold was set for GFP^+ areas. A comparison to control images taken with a red filter set was used to control for autofluorescence. Identical settings were used between animal groups for a given organ.

H&E staining was performed according to standard protocols on paraffin sections.

Vector Biodistribution

Tissue DNA was extracted with QIAamp DNA Mini Kit (QIAGEN, CA), and vector genomes were quantified by real-time PCR using Taqman reagents (Applied Biosystems, Life Technologies, CA) and primer/probe targeting the rBG polyadenylation sequence of the vectors.

Statistics

GFP quantification results and vector genome copies in mice were analyzed using one-way ANOVA (Kruskal Wallis test) followed by Dunn's multiple comparisons test with an alpha value of 0.05 (GraphPad Prism).

Supplemental References

1. Patrick, D, and Rebelatto, M (2015). Toxicologic pathology and background lesions of nonhuman primates In: Bluemel, J, Korte, S, Schenck, E and Weinbauer, G (eds). *The Nonhuman Primate in Nonclinical Drug Development and Safety Assessment*. G. Elsevier. pp 245-252.
2. Deverman, B.E., Pravdo, P.L., Simpson, B.P., Kumar, S.R., Chan, K.Y., Banerjee, A., Wu, W.-L., Yang, B., Huber, N., Pasca, S.P., and Gradinaru, V.ea (2016). Cre-dependent selection yields AAV variants for widespread gene transfer to the adult brain. Nat Biotechnol. 34, 204–209 34.
3. Lock, M., Alvira, M., Vandenberghe, L.H., Samanta, A., Toelen, J., Debyser, Z., and Wilson, J.M. (2010). Rapid, simple, and versatile manufacturing of recombinant adeno-associated viral vectors at scale. Hum. Gene Ther. 21, 1259–1271.
4. Lock, M., Alvira, M.R., Chen, S.J., and Wilson, J.M. (2014). Absolute determination of single-stranded and self-complementary adeno-associated viral vector genome titers by droplet digital PCR. Hum. Gene Ther. Methods 25, 115–125.